Journal of General Virology (2016), **97**, 246–257 **DOI** 10.1099/jgv.0.000323

Tobacco rattle virus 16K silencing suppressor binds ARGONAUTE 4 and inhibits formation of RNA silencing complexes

Lourdes Fernández-Calvino,[1] Llúcia Martínez-Priego,[1] Edit Z. Szabo,[2] Irene Guzmán-Benito,[1] Inmaculada González,[1] Tomás Canto,[1] Lóránt Lakatos[2,3] and César Llave[1]

Correspondence
César Llave
cesarllave@cib.csic.es

[1]Department of Environmental Biology, Centro de Investigaciones Biológicas, Consejo Superior de Investigaciones Científicas, Ramiro de Maeztu 9, 28040 Madrid, Spain

[2]Department of Dermatology and Allergology, University of Szeged, H-6720 Szeged, Koranyi str. 6, Hungary

[3]MTA-SZTE Dermatological Research Group, Hungary

Received 15 June 2015
Accepted 20 October 2015

The cysteine-rich 16K protein of tobacco rattle virus (TRV), the type member of the genus *Tobravirus,* is known to suppress RNA silencing. However, the mechanism of action of the 16K suppressor is not well understood. In this study, we used a GFP-based sensor strategy and an *Agrobacterium*-mediated transient assay in *Nicotiana benthamiana* to show that 16K was unable to inhibit the activity of existing small interfering RNA (siRNA)- and microRNA (miRNA)-programmed RNA-induced silencing effector complexes (RISCs). In contrast, 16K efficiently interfered with *de novo* formation of miRNA- and siRNA-guided RISCs, thus preventing cleavage of target RNA. Interestingly, we found that transiently expressed endogenous miR399 and miR172 directed sequence-specific silencing of complementary sequences of viral origin. 16K failed to bind small RNAs, although it interacted with ARGONAUTE 4, as revealed by bimolecular fluorescence complementation and immunoprecipitation assays. Site-directed mutagenesis demonstrated that highly conserved cysteine residues within the N-terminal and central regions of the 16K protein are required for protein stability and/or RNA silencing suppression.

INTRODUCTION

Tobacco rattle virus (TRV) is a bipartite, positive-sense ssRNA plant virus and the type member of the genus *Tobravirus* (family *Virgaviridae*) (Macfarlane, 2010). TRV is an important pathogen of cultivated potato, although it infects a wide range of plant species, including the model plants *Nicotiana benthamiana* and *Arabidopsis thaliana* (Fernández-Calvino *et al.*, 2014).

TRV infection is tightly controlled by RNA silencing, as deduced by elevated TRV levels in plants in which RNA silencing components are genetically inactivated (Donaire *et al.*, 2008). ARGONAUTE (AGO) proteins are core components of RNA-induced silencing effector complexes (RISCs), which use small RNA (sRNA) to silence complementary RNA through translational repression and/or RNA slicing (Brodersen & Voinnet, 2006; Vaucheret, 2008). A programmable small interfering RNA (siRNA)-containing antiviral AGO complex is triggered upon TRV infection to selectively cleave viral RNA (Ciomperlik *et al.*, 2011). Several studies have identified the TRV-encoded 16K protein as the main suppressor of RNA silencing (Ghazala *et al.*, 2008; Martín-Hernández & Baulcombe, 2008; Martínez-Priego *et al.*, 2008), although the 29K movement protein also contributes to suppression of RNA silencing in the context of virus replication (Deng *et al.*, 2013). 16K is primarily cytoplasmic, although it can be found to a lesser extent in the nucleus, coinciding with the existence of two functional bipartite nuclear localization signals in the protein (Ghazala *et al.*, 2008; Liu *et al.*, 1991). In plants, 16K suppresses RNA silencing induced by ssRNA as well as by a low concentration of dsRNA, and reduces the accumulation of siRNAs in both transient and stable expression assays (Ghazala *et al.*, 2008; Martín-Hernández & Baulcombe, 2008; Martínez-Priego *et al.*, 2008). Interestingly, TRV accumulates and propagates systemically without 16K in WT plants (Deng *et al.*, 2013; Martín-Hernández & Baulcombe, 2008). However, TRV mutants carrying a dysfunctional 16K gene exhibit appreciable differences in their accumulation dynamics with respect to the WT virus (Deng *et al.*, 2013), cause

One supplementary table is available with the online Supplementary Material.

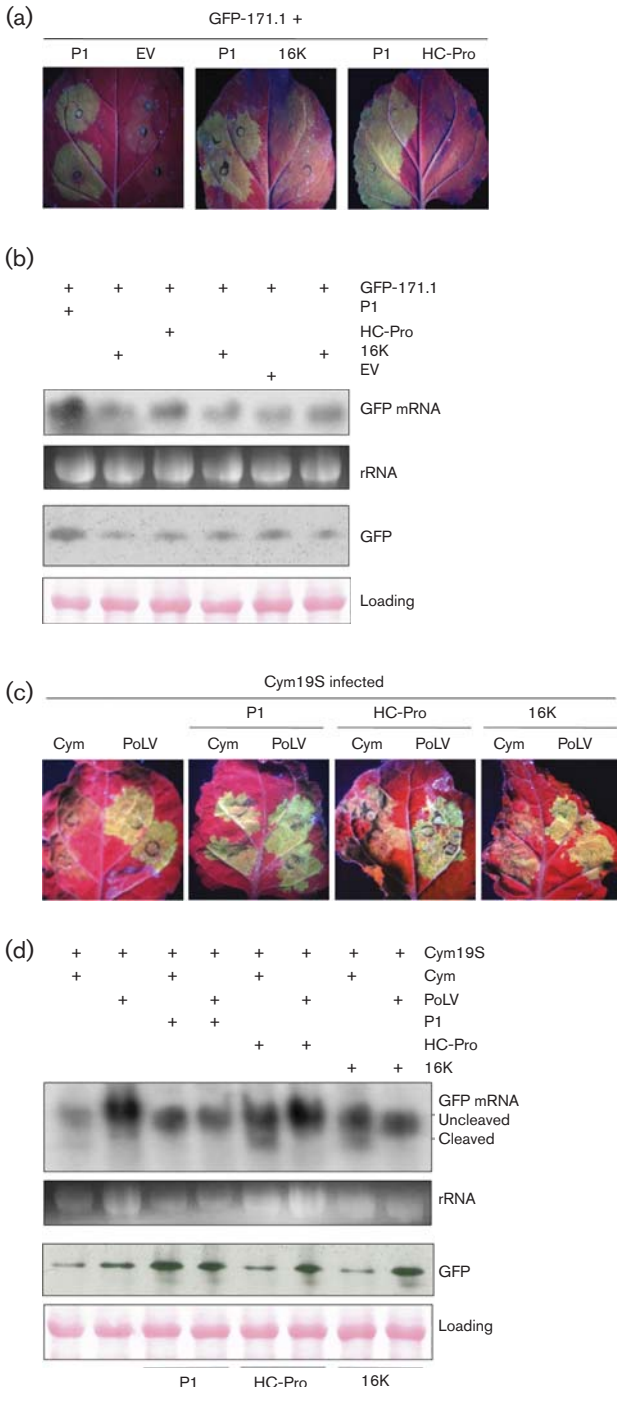

Fig. 1. 16K does not interfere with the activity of miRNA and viral siRNA pre-assembled RISCs. (a) GFP-171.1 was agroinjected with 16K or empty vector (EV). SPMMV P1 and TEV HC-Pro were used as positive and negative controls, respectively. GFP fluorescence was monitored under UV light at 3 days p.i. (b) Northern and Western blot analyses in patches infiltrated with GFP171.1 and constructs expressing silencing suppressors or EV as indicated. (c) GFP fluorescence of Cym19S-infected recovering leaves infiltrated with GFP–Cym (Cym) or GFP–PoLV (PoLV) sensors and silencing suppressors. (d) Northern and Western blot analyses in Cym19S-infected recovering leaves infiltrated with GFP–Cym or GFP–PoLV sensors and silencing suppressors as indicated. RNA blots were hybridized with DNA radiolabelled probes. Immunoblots were incubated with polyclonal anti-GFP. Ethidium bromide-stained rRNA and Red Ponceau staining were used as RNA and protein loading controls, respectively.

necrotic symptoms in inoculated and systemically infected leaves (Deng *et al.*, 2013; Martín-Hernández & Baulcombe, 2008) and are unable to invade meristems (Martín-Hernández & Baulcombe, 2008). In addition, 16K supports synergistic effects on virus double infections (Andika *et al.*, 2012) and contributes to stabilizing the genomic RNA2 of TRV (Deng *et al.*, 2013). In this study, we wanted to gain insights into the mechanism of suppression of 16K using an *Agrobacterium*-mediated transient assay in *N. benthamiana.*

RESULTS

16K does not inhibit the activity of miRNA- and viral siRNA-programmed RISCs

To investigate whether 16K inhibits active (assembled) miRNA-loaded RISC complexes, we used an *Agrobacterium*-mediated transient assay in *N. benthamiana* to express a GFP-based sensor construct, driven by the 35S cauliflower mosaic virus promoter, with or without viral suppressor. The GFP-171.1 sensor contained a full complementary miR171-binding site immediately downstream of the stop codon of GFP, allowing miR171-mediated silencing of the GFP-171.1 mRNA (Parizotto *et al.*, 2004). GFP expression in the infiltrated zone was compared with that of leaves in which GFP-171.1 was co-infiltrated with tobacco etch potyvirus (TEV) HC-Pro or sweet potato mild mottle ipomovirus (SPMMV) P1 silencing suppressor, which was used as control. HC-Pro has no effect on miRNA- and siRNA-loaded RISCs, whereas P1 inhibits miRNA-programmed RISC activity (Giner *et al.*, 2010; Lakatos *et al.*, 2006). In our assays, GFP fluorescence was detected under UV light at comparable low levels in leaves infiltrated with 16K, HC-Pro or empty vector at 2 days post-infiltration (p.i.) (Fig. 1a). In contrast, leaves agroinjected with P1 showed a marked increase in green fluorescence as a result of P1-mediated interference on miR171-guided cleavage of the GFP-171.1 mRNA (Fig. 1a). GFP-171.1 mRNA and protein accumulated to the same levels in samples injected with 16K, HC-Pro or empty vector, whereas they accumulated to higher levels when P1 was co-delivered in the patch (Fig. 1b). Therefore, 16K, like HC-Pro, failed to inhibit the activity of miR171-loaded active RISCs.

Next, we wondered whether 16K might inhibit viral siRNA-loaded active silencing complexes. To test this

possibility, we used plants infected systemically with a Cymbidium ringspot tombusvirus (CymRSV) 19 Stop mutant (Cym19S), which does not express the P19 silencing suppressor (Szittya *et al.*, 2002). These plants display a phenotype of recovery due to the activation of a strong RNA silencing response that implicates the processing activity of viral siRNA-loaded AGO complexes against the virus (Silhavy *et al.*, 2002; Szittya *et al.*, 2002). The sensor construct GFP–Cym, which contains an ~200 bp portion of the CymRSV RNA fused after the GFP stop codon, is susceptible to cleavage by RISCs containing viral siRNAs (Giner *et al.*, 2010; Lakatos *et al.*, 2006). The GFP–PoLV construct, in which GFP is fused with an ~200 bp portion of pothos latent aureusvirus (PoLV), was used as a negative control (Pantaleo *et al.*, 2007). Recovering leaves of Cym19S-infected plants were then infiltrated with GFP–Cym or GFP–PoLV alone or with the indicated silencing suppressors. Visual inspection of GFP fluorescence showed that GFP–Cym, but not the non-target GFP–PoLV sensor, was downregulated by RNA silencing against Cym19S (Fig. 1c). Moreover neither HC-Pro nor 16K was able to elevate the accumulation of the cognate sensor (GFP–Cym), while patches infiltrated with the non-cognate sensor showed much brighter fluorescence. In contrast, GFP fluorescence was strong in patches infiltrated with GFP–Cym or GFP–PoLV together with P1, indicating suppression of RNA silencing (Fig. 1c).

Co-expression of the GFP–Cym construct with 16K or HC-Pro in infected leaves resulted in the accumulation of full-length mRNA along with a shorter 3′ RNA cleavage product that originated from viral siRNA-directed processing of the complementary region in the GFP–Cym mRNA (Fig. 1d). In contrast, a unique hybridization band corresponding to the intact full-length mRNA was detected in tissues injected with the non-homologous GFP–PoLV (Fig. 1d). Accordingly, GFP–PoLV protein levels were higher than the GFP–Cym levels (Fig. 1d). Therefore, 16K was not competent to interfere with viral siRNA-programmed active RISCs and to prevent cleavage of the GFP–Cym sensor RNA. GFP mRNA and protein levels were similar in samples injected with GFP–Cym or GFP–PoLV in the presence of P1, which is known to inhibit the slicing activity of viral siRNA-containing AGO complexes (Fig. 1d). Furthermore, no cleavage products of GFP were found in samples co-infiltrated with the GFP–Cym and P1 constructs.

16K interferes with *de novo* formation of RISCs and target cleavage

We investigated whether 16K interferes with RISC assembly to prevent subsequent target cleavage using two possible targeting scenarios: host sequences and viral sequences (Kasschau *et al.*, 2003). We used a GFP-based sensor strategy to test functional miRNA–target interactions. Given that miR171-containing AGO complexes exist in the *N. benthamiana* leaves prior to agroinfiltration, we generated a novel reporter to test this hypothesis. The validated binding site of miR172 as found in *APETALA2* (*AP2*) (Chen, 2004) was placed immediately after the GFP ORF stop codon (Fig. 2a). The resultant GFP–AP2 construct was agroinjected either alone, with an empty vector or with a miRNA gene. The observation of bright fluorescence in patches containing GFP–AP2 and empty vector validated our sensor assay and ruled out a potential regulatory effect driven by pre-assembled endogenous miR172 (Fig. 2b). When GFP–AP2 was delivered in the presence of empty vector or heterologous miRNAs (miR399, miR158 or miR171), GFP fluorescence and GFP–AP2 transcript levels in the infiltrated zone were comparable to those of a native GFP construct (Fig. 2b, c). In contrast, the fluorescence virtually disappeared and GFP–AP2 mRNA remained below detection limits when the GFP–AP2 sensor was co-injected with the cognate miR172-expressing construct, presumably due to miR172-mediated cleavage of the GFP–AP2 mRNA (Fig. 2b, c). Interestingly, restoration of green fluorescence and GFP–AP2 mRNA levels in the presence of 16K or HC-Pro indicated that miR172-guided silencing was partially abolished (Fig. 2b, c). These results suggested that 16K interferes with the proper formation and subsequent function of AGO-containing effector complexes.

Next, we tested the ability of 16K to perturb host miRNA programming and targeting against viral sequences. To test this idea, we first investigated whether host miRNAs promote endonucleolytic cleavage of complementary viral sequences. We took advantage of our validated miR172-targeting system, and hence the mature miR172 sequence was used as a query to search for potential targets in a collection of viral genomes using the Small RNA Target Prediction program (Jones-Rhoades & Bartel, 2004). This analysis identified the genome of maize chlorotic dwarf sequivirus (MCDV) as comprising potential miR172-binding sites (Fig. 3a). We also searched for host miRNAs that base pair with the TRV genome and identified miR399 as a candidate interactor (Fig. 3a).

A stretch of 30 nt harbouring each of the target viral sequences was fused to the GFP ORF immediately after the stop codon. The resulting GFP–MCDV and GFP–TRV constructs were expressed either alone or in combination with miRNA-containing constructs as shown above. Green fluorescence was detected in patches infiltrated with GFP–MCDV plus empty vector or heterologous miRNAs (miR399, miR158 and miR171) to levels similar to those observed in tissue expressing the WT GFP alone (Fig. 3b). This finding excluded a potential effect of pre-assembled miR172-guided complexes against GFP–MCDV transcripts. In contrast, GFP expression was turned off when GFP–MCDV was co-delivered with a miR172-containing construct (Fig. 3b). GFP–MCDV mRNA was drastically diminished in the presence of miR172 owing to miR172-triggered post-transcriptional silencing (Fig. 3b). Green fluorescence was observed in patches containing GFP–TRV and empty vector or

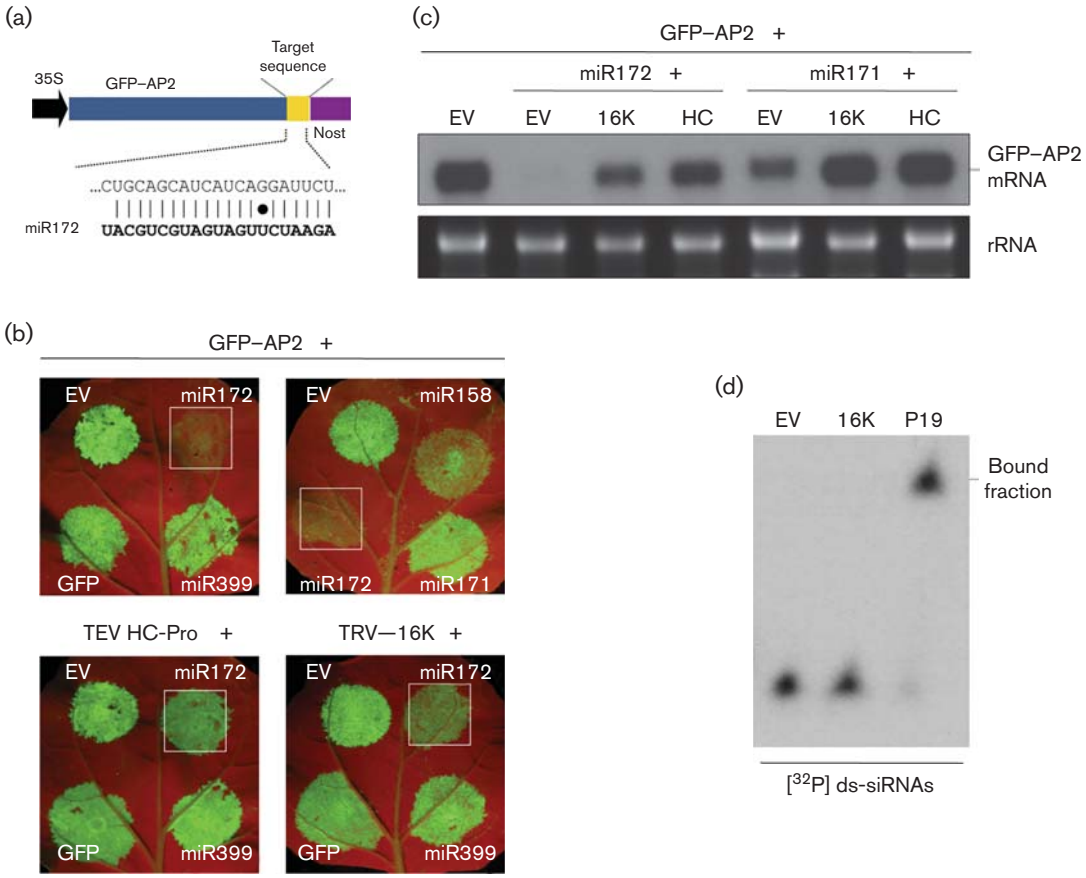

Fig. 2. 16K interferes with assembly of miRNA-guided RISCs. (a) Diagrammatic representation of the miR172 complementary region within the 35S-driven GFP–AP2. The miRNA sequence and partial sequence of the validated target mRNA are shown in the expanded area. G : U base pairing is shown (black dot). Nost, nopaline synthase (NOS) terminator. (b) GFP fluorescence (3 days p.i.) in leaves co-infiltrated with GFP–AP2 and each of the miRNA-containing constructs indicated. Patches injected with the cognate miR172 are outlined with an open box. An empty vector (EV) was used as a negative suppression control. Spots labelled as GFP were infiltrated with a GFP-coding construct alone and were used as controls of fluorescence. Infiltration assays with TEV HC-Pro or 16K are shown. (c) Northern blot assays of GFP–AP2 mRNA in patches co-infiltrated with GFP–AP2 and miR172- or miR171-containing constructs in the presence of 16K, TEV HC-Pro (positive control) or EV (negative control). A GFP DNA radiolabelled probe was used. Ethidium bromide-stained rRNA (prior to transfer) is shown as a loading control. (d) Gel mobility shift assay for protein–siRNA interactions. Crude protein extracts were incubated with synthetic radiolabelled, 21 nt double-stranded (ds)-siRNAs. Leaves injected with P19 and EV were used as positive and negative controls, respectively.

heterologous miRNAs (miR158 and miR171), but was notably reduced when GFP–TRV was co-delivered with miR399 (Fig. 3c). Accordingly, GFP–TRV mRNA accumulated to a lower level if miR399 was co-expressed in the agroinfiltrated leaves (Fig. 3c). As would be anticipated, both 16K and HC-Pro interfered with *de novo* formation of miRNA complexes and suppressed miRNA-mediated silencing, irrespective of the origin of the target sequences, restoring green fluorescence derived from GFP–MCDV to nearly WT levels (Fig. 3b).

Selective binding to sRNAs represents the basis for inhibition of RISC assembly and target cleavage by multiple viral proteins (Lakatos *et al.*, 2006). We examined *in vitro* whether 16K was capable of binding ds-sRNAs. Crude extracts of *N. benthamiana* leaves expressing a silencing suppressor-competent 16K were incubated with ^{32}P-labelled synthetic 21 nt ds-siRNAs, and the complexes were resolved on a native electrophoresis gel. P19 from tomato bushy stunt tombusvirus (TBSV) was used as a binding control. As expected, the P19 control bound dsRNA as evidenced by a shift in siRNA mobility due to the formation of P19–siRNA complexes (Fig. 2d). No siRNA binding could be inferred from leaves expressing either empty vector or 16K (Fig. 2d).

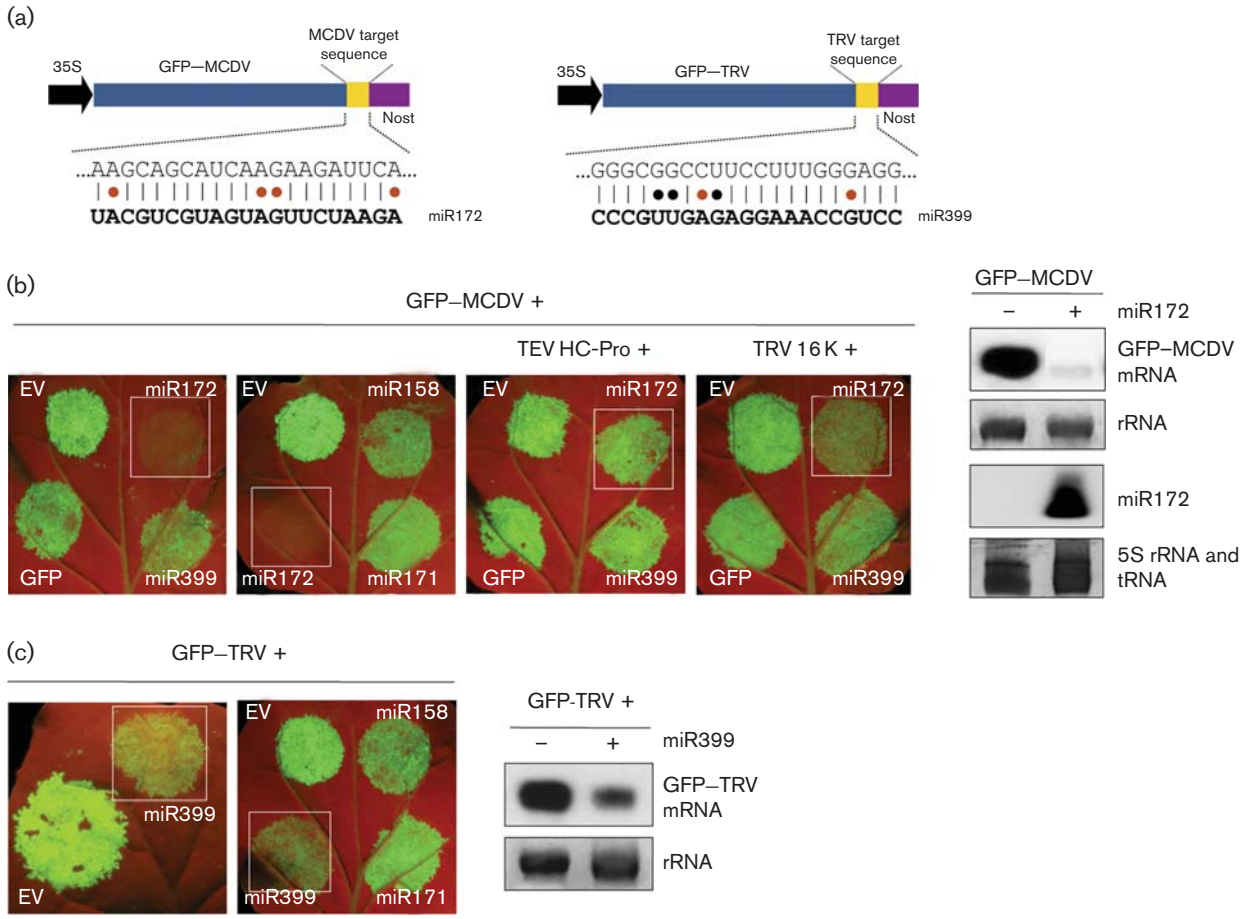

Fig. 3. Host-encoded miRNAs target viral sequences for silencing. (a) Schematic representation of target mRNA complementary regions within the 35S-driven GFP–MCDV and GFP–TRV constructs. The miRNA sequence and partial sequence of the predicted target viral RNA are shown in the expanded area. Mismatched (red dots) and G : U (black dots) base pairings are shown. Nost, NOS terminator. (b) Left: GFP fluorescence (3 days p.i.) in patches co-infiltrated with GFP–MCDV and each of the miRNA-containing constructs indicated. Patches injected with miR172 are outlined with an open box. An empty vector (EV) was used as a negative control. A GFP-expressing construct was used as a control of fluorescence. Infiltration assays with TEV HC-Pro or 16K are shown. Right: Northern blot assays of GFP–MCDV mRNA and miR172 in patches co-infiltrated with GFP–MCDV and EV (−) or miR172 (+). RNA blots were hybridized with radiolabelled probes complementary to GFP or miR172. Ethidium bromide-stained RNA (prior to transfer) is shown as a loading control. (c) Left: GFP fluorescence in leaf patches co-infiltrated with a GFP–TRV sensor construct and each of the miRNA-containing constructs indicated. Patches injected with miR399 are outlined with an open box. Infiltration assays were conducted as in (b). Right: Northern blot assays of GFP–TRV mRNA in patches co-infiltrated with GFP–TRV and EV (−) or miR399 (+).

16K physically interacts with AGO4

To test whether the 16K silencing suppressor interacts physically with AGO proteins, we used bimolecular fluorescence complementation (BiFC) to monitor *in vivo* protein–protein interactions. When proteins tagged with the N-terminal half of the split yellow fluorescent protein (sYFPN) were co-infiltrated with an empty construct containing the C-terminal half of the sYFP (sYFPC), or when the sYFPC-tagged proteins were co-expressed with a construct expressing sYFPN alone, no fluorescence could be detected (data not shown). At 3 days p.i., we found that the 16K protein interacted strongly with itself in *N. benthamiana* epidermal cells. The fluorescence derived from the reconstitution of the YFP fluorophore was predominantly cytoplasmic, although nucleolus-associated fluorescence was detected within the nucleus (Fig. 4a). Our BiFC assay revealed reconstitution of the YFP fluorophore, mostly localized in the cytoplasm, in samples co-agroinjected with sYFPN–16K and sYFPC–AGO1, suggesting a 16K–AGO1 association (Fig. 4b). However, AGO1 binding could not be validated by immunoprecipitation (IP) assays using different tagged-protein combinations (data not

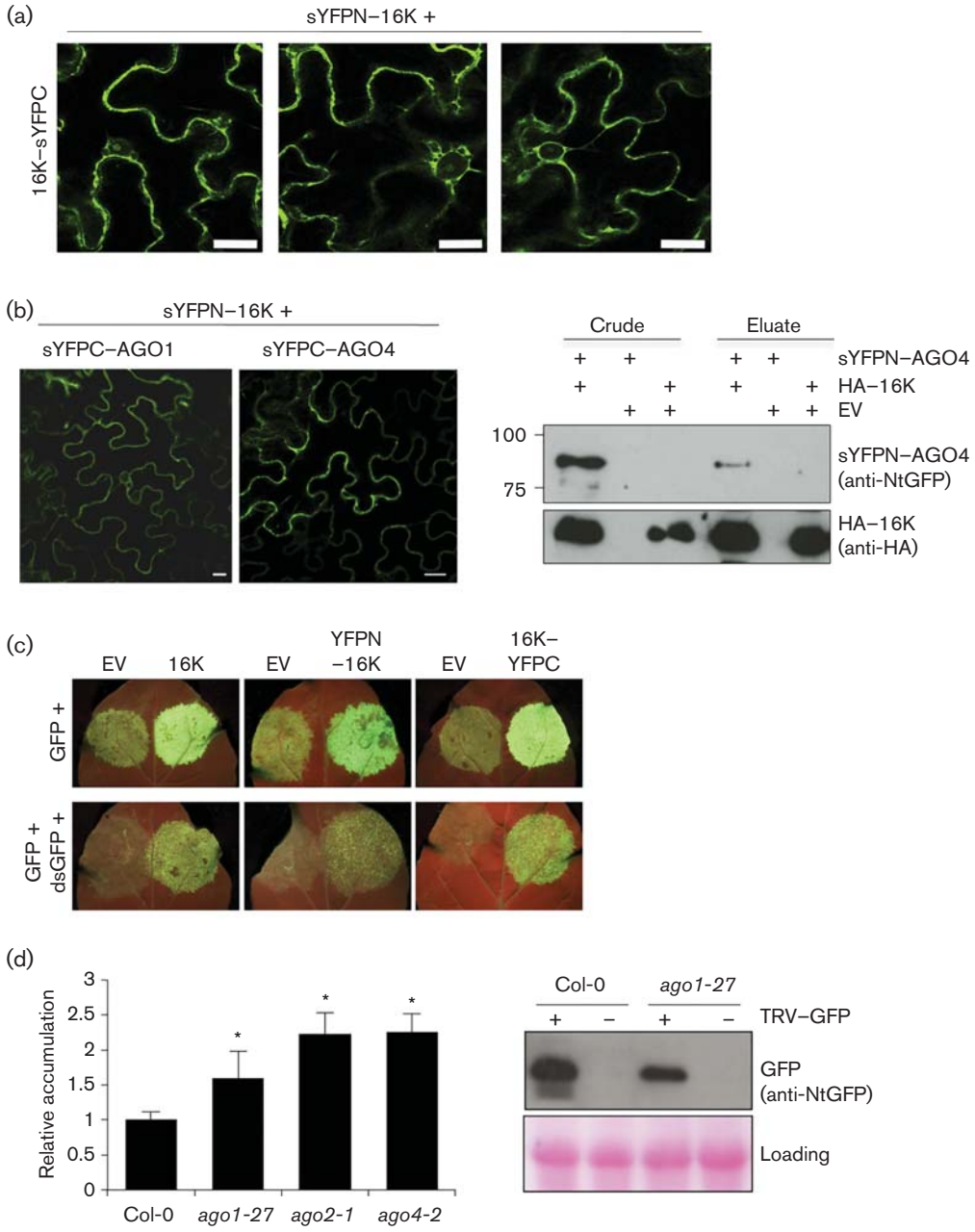

Fig. 4. Analysis of 16K self-interaction and AGO binding. (a) Visualization of the distribution of fluorescence derived from BiFC in epidermal cells expressing sYFP-tagged 16K proteins. (b) Left: BiFC-derived fluorescence in tissue co-expressing sYFP-tagged 16K and AGO1 or AGO4 proteins as indicated. Bars, 75 μm. Right: haemagglutinin (HA)-tagged 16K proteins were immunoprecipitated from leaves co-expressing HA–16K and sYFPN–AGO4. Western blotting was done using an N-terminal half GFP (anti-NtGFP) antibody to detect sYFPN–AGO4 and anti-HA antibody to detect HA–16K. (c) The silencing suppressor activity of sYFP-tagged 16K constructs was assessed in leaves co-expressing GFP or GFP plus dsGFP at 5 days p.i. An HA-tagged 16K and empty vector (EV) were used as a positive and negative suppression controls, respectively. (d) Left: TRV RNA1 accumulation determined by qRT-PCR in TRV-infected *ago1-27*, *ago2-1* and *ago4-2*. Expression values are relative to that in Arabidopsis ecotype Columbia (Col-0), which was arbitrarily set to 1.Asterisks indicate statistical significance versus the control (*$P<0.001$, Duncan's multiple range test). Right: TRV-derived GFP accumulation determined by Western blotting using an anti-NtGFP antibody. Red Ponceau staining was used as a protein loading control.

shown). Interestingly, BiFC suggested a cytoplasmic association of 16K with AGO4 that was further validated by IP using a haemagglutinin (HA)-tagged version of 16K and an sYFPN–AGO4 construct (Fig. 4b). At 3 days p.i., extracts were prepared from infiltrated leaves and HA-tagged 16K was immunoprecipitated with an anti-HA antibody. The 16K protein was detected by Western blotting using an anti-HA antibody in all samples tested, indicating that HA–16K could be immunoprecipitated from extracts (Fig. 4b). Using an anti-GFP antibody, we found that sYFPN–AGO4 co-immunoprecipitated with HA–16K, confirming that the interaction was specific (Fig. 4b).

To test whether sYFP tagging of 16K affected its ability to suppress local silencing, we analysed the sYFPN–16K and sYFPC–16K constructs used in BiFC in a transient GFP-based silencing assay. Patches infiltrated with GFP and sYFPN–16K or sYFPC–16K showed a marked increase in green fluorescence that was comparable to that observed in the presence of the native 16K protein (Fig. 4c). Furthermore, suppression of GFP silencing was also evident upon transient co-expression of GFP with an inverted-repeat dsGFP construct, demonstrating that sYFP tagging of 16K did not compromise its silencing suppression properties (Fig. 4c).

Mutations of conserved cysteines of 16K affect protein accumulation and silencing suppressor activities

The 16K gene of tobraviruses encodes a protein with N-terminal and central Cys-rich motifs reminiscent of zinc-finger domains present in some regulatory proteins (Fig. 5a) (Liu *et al.*, 2002). Comparison of 16K with other Cys-rich proteins from furoviruses, hordeiviruses and pecluviruses identified a central highly conserved Cys-Cys-Gly-X-X-His pattern (Fig. 5a) (Diao *et al.*, 1999). We wanted to investigate the significance of the Cys residues within the conserved N-terminal and central motifs of 16K on protein stability, silencing suppression and AGO4 binding. We used site-directed mutagenesis to generate: (i) a 16K deletion mutant that lacked the Cys-containing first N-terminal 17 aa, and (ii) a double 16K mutant in which Cys at aa 65 and 66 was replaced with phenylalanine (Fig. 5a). The resulting 16KΔ17 and 16KC65-66/P mutants were fused to sYFPN to create sYFPN–16KΔ17 and sYFPN–16KC65-66/P recombinant proteins, respectively.

We first investigated whether the sYFPN–16K mutant proteins retained the ability to block intrinsic silencing triggered by T-DNA expression. The silencing suppressor activity of the sYFPN-tagged 16K mutants was compared with sYFPN–16K using an agroinfiltrated patch silencing suppression assay in *N. benthamiana* at 5 days p.i. Northern blotting revealed a subtle increased in GFP transcripts in patches co-infiltrated with GFP and sYFPN–16KΔ17 and sYFPN–16KC65-66/P compared with control plants injected with empty vector, suggesting a partial inhibition of GFP silencing (Fig. 5b). However, the extent to which GFP silencing was suppressed by both mutants was far less than that observed in plants infiltrated with the native sYFPN–16K (Fig. 5b). Visual inspection under UV light at 5 days p.i. revealed decreased green fluorescence in patches co-infiltrated with GFP and sYFPN–16KΔ17, sYFPN–16KC65-66/P or empty vector relative to sYFPN–16K (Fig. 5c).

To test whether the above mutations affected protein stability, we compared accumulation of 16K mutant proteins relative to WT 16K. The sYFPN-tagged 16K-derived constructs were agroinfiltrated at a culture OD_{600} of 0.1 or 0.3 and proteins were extracted at 3 days p.i. and analysed by Western blotting using the N-terminal half GFP antibody. Densitometric analysis of several independent replicates revealed that sYFPN–16KC65-66/P accumulated at a level 40–70 % less than the sYFPN–16K control (a representative blot is shown in Fig. 5d). In most cases, the accumulation of sYFPN–16KΔ17 in the transient assay was reduced by nearly 40 % compared with sYFPN–16K, although we occasionally detected similar protein accumulation in leaves infiltrated with sYFPN–16K or sYFPN–16KΔ17 (Fig. 5e). Low protein levels in our assay could be interpreted as protein instability caused by the 16KΔ17 and C65-66/P mutations. Alternatively, it could be a consequence of the mutants' inability to suppress local silencing triggered by T-DNA expression. We found that sYFPN–16KΔ17 protein levels were significantly elevated when a functional P19 suppressor was transiently co-delivered, indicating that the suppressor-deficient sYFPN–16KΔ17 protein was stable provided that silencing was counteracted by P19 (Fig. 5e). This finding suggests that the failure of sYFPN–16KΔ17 to suppress local transgene silencing causes a negative-feedback inhibition on its own production, which in turn leads to reduced GFP expression. In contrast, sYFPN–16KC65-66/P proteins remained at low levels irrespective of P19, pointing to a dramatic impact of this mutation on protein accumulation that indirectly results in a dysfunctional suppressor of silencing (Fig. 5e).

We failed to detect YFP fluorescence derived from the BiFC of transiently expressed sYFPN–16K mutants and sYFPC–AGO4 (Fig. 5f). Likewise, we could not appreciate self-association of sYFPN- and sYFPC-tagged 16K mutant constructs (data not shown). Given that both C65-66/P and 16KΔ17 mutations affected protein accumulation, we cannot unambiguously discriminate whether the lack of BiFC-derived YFP fluorescence was due to poor protein levels in the injected tissue or the inability of mutated proteins to interact.

The 16K suppressor of TRV possesses a single glycine/tryptophan (GW) motif at position 48 within the N-terminal half. GW/WG repeats have been identified in viral suppressors of silencing, and they can act as AGO hooks essential for AGO binding (Azevedo *et al.*, 2010; Giner *et al.*, 2010; Karlowski *et al.*, 2010). Using a 16K construct carrying a

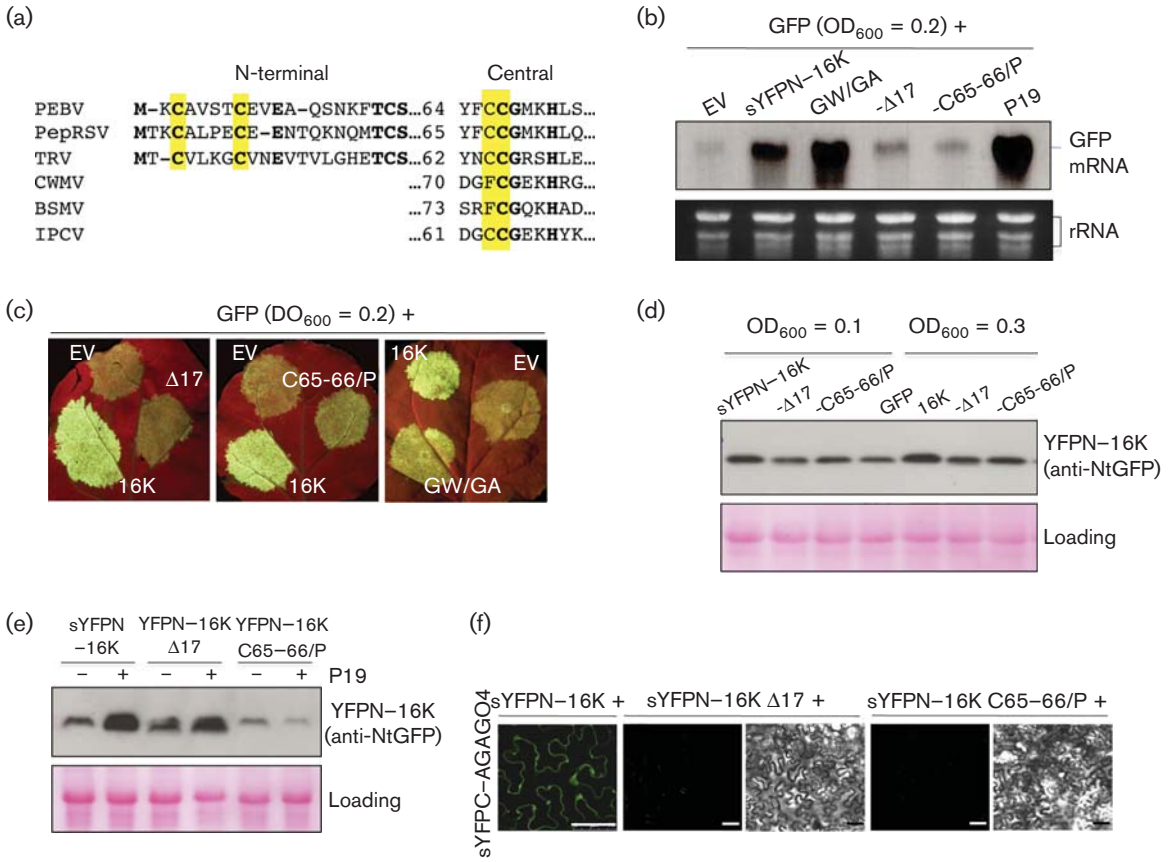

Fig. 5. Effect of mutations on conserved Cys-rich motifs within the N terminus of 16K on protein accumulation and silencing suppression. (a) Alignment of partial amino acid sequences of Cys-rich viral proteins: tobravirus (PEBV, pea early browning virus; PepRSV, pepper ring spot virus; TRV) 16K proteins, furovirus (CWMV, Chinese wheat mosaic virus) 19K protein, hordeovirus (BSMV, barley stripe mosaic virus) γb protein and pecluvirus (IPCV, Indian peanut clump virus) RNA1 3′ terminal gene. The amino acids tested are highlighted in yellow; those common to all sequences are in bold. (b, c) Silencing suppressor activity of sYFPN-tagged 16K constructs in a local transient assay. GFP was co-infiltrated with empty vector (EV) or sYFPN-tagged 16K derivatives as indicated. A Northern blot of GFP mRNA was analysed using a GFP-radiolabelled probe at 5 days p.i. EV and P19 were used as negative and positive suppression controls, respectively. Ethidium bromide-stained RNA (prior to transfer) is shown as a loading control (b). (c) GFP fluorescence was monitored under UV light at 5 days p.i. (d) Western blot of sYFPN-tagged 16K proteins in agroinoculated leaves at 3 days p.i. using an anti-NtGFP antibody. Red Ponceau staining was used as a protein loading control. (e) Western blot of sYFPN-tagged 16K constructs in the presence of empty vector (−) or P19 (+). (f) BiFC assay between sYFPN-tagged 16K derivatives and sYFPC–AGO4 proteins. No BiFC-derived fluorescence was observed. A positive control using sYFPN–16K is shown. Bars, 75 μm (16K); 50 μm (16K mutants).

GW→GA point mutation, we found that this predicted GW motif was irrelevant for silencing suppressor in the transient assay (Fig. 5b, c).

DISCUSSION

In this study, we aimed to better understand the molecular basis of the 16K-mediated inhibition of RNA silencing. Our results indicated that, in the transient assay, 16K was unable to block cleavage of a GFP sensor mRNA by a pre-existing miRNA/siRNA-programmed RISC. However, 16K successfully prevented miRNA-guided cleavage of target RNAs when both the miRNA and the sensor constructs were co-delivered simultaneously into the plant tissue. This suggested that 16K presumably acted by impeding initial RISC assembly. The P19, p21 and HC-Pro viral suppressors, which primarily block RISC programming, use sRNA sequestration as a means to prevent sRNA incorporation into AGO (Burgyán & Havelda, 2011; Garcia-Ruiz *et al.*, 2015; Lakatos *et al.*, 2006; Schott *et al.*, 2012). As opposed to these suppressors, the basis for the inhibition of RISC formation by 16K was not related to sRNA sequestration as 16K failed to bind siRNAs. However, it is conceivable that 16K could affect RISC assembly by compromising sRNA availability as 16K causes reduced

accumulation of silencing-associated siRNAs (Ghazala *et al.*, 2008; Martínez-Priego *et al.*, 2008). Alternatively, 16K could perturb RISC assembly by interfering with AGO proteins. Our BiFC assay suggested a potential interaction between 16K and AGO1, although this could not be validated by IP. In contrast, we found compelling evidence that 16K associates with AGO4. miR172 harbours a 5′-terminal adenosine and binds AGO4 to direct effective cleavage of *AP2* mRNA targets *in vitro* (Qi *et al.*, 2006). These findings suggest a productive role for AGO4 in our transient silencing assay. However, whether 16K interferes with *de novo* formation of RISC via AGO4 binding remains to be tested.

Here, we found roles for AGO2 and AGO4 in susceptibility to TRV, whereas AGO1 targeting of TRV is unclear, as suggested by the erratic accumulation of TRV in *ago1-27* mutants observed using quantitative reverse transcription (qRT)-PCR and Western blotting (Fig. 4d). These observations have been corroborated recently by others (Carbonell & Carrington, 2015; Ma *et al.*, 2015) and suggest that AGO2 and AGO4 are the two major antiviral AGOs against TRV. The question raised is whether 16K association with AGO4 alleviates antiviral effects during TRV infection. Despite AGO4 normally functioning in transcriptional gene silencing by guiding hypermethylation of target DNA, it plays an antiviral role against several RNA viruses that is probably related to RNA slicing (Carbonell & Carrington, 2015). Direct physical interaction of viral silencing suppressors with AGO4 has been reported, consistent with their ability to block the *in vitro* slicer activity of AGO4 (Hamera *et al.*, 2012; Pérez-Cañamás & Hernández, 2015). Furthermore, AGO4-mediated cleavage-independent control of virus translation has been shown to modulate virus resistance induced by NB-LRR protein in *N. benthamiana* (Bhattacharjee *et al.*, 2009).

The 16K protein is a small Cys-rich protein that shares sequence homology with Cys-rich proteins of members of the genera *Furovirus*, *Hordeivirus*, *Pecluvirus*, *Benyvirus* and *Carlavirus*. In complementation studies, the soilborne wheat mosaic furovirus (SBWMV) 19K or the barley stripe mosaic hordeivirus (BSMV) γb protein functionally replaced the 16K of TRV, indicating that Cys-rich proteins probably share common functions (Liu *et al.*, 2002). In fact, BSMV γb, SBWMV 19K and peanut clump pecluvirus 15K proteins are known to suppress RNA silencing and modulate symptom severity and systemic virus accumulation (Donald & Jackson, 1994; Dunoyer *et al.*, 2002; Te *et al.*, 2005; Yelina *et al.*, 2002). We found that the highly conserved Cys residues at the N-terminal segment of 16K were critical for protein stability and function. Whereas the lack of suppression by sYFPN–16KC65-66/P was probably due to protein instability incurred by the double C65-66/P mutation, the 16KΔ17 deletion rendered a suppression-deficient protein that was unable to repress local silencing triggered by T-DNA expression. It would be interesting to test whether mutations of these conserved Cys residues disrupted the formation of the zinc-finger structure leading to improper protein folding. In addition, future research should be conducted to determine the effects of Cys mutations in the context of TRV infection.

Our results depict a scenario whereby host sRNAs hold the potential to downregulate viral genomes (Lin *et al.*, 2009; Llave, 2004; Niu *et al.*, 2006; Simón-Mateo & García, 2006). We proved that miR172 and miR399 dampen expression of GFP sensors carrying complementary sequences from MCDV and TRV genomes, respectively. It is worth noting that the selected miR172 : GFP–MCDV RNA duplex has only moderate complementarity, with two central mismatches. This indicates that perfect central complementarity is not compulsory for target recognition and mRNA clearing, and that factors others than sequence complementarity at the binding site could influence the outcome of silencing. This agrees with a recent paper by Li *et al.* (2014) in which they demonstrated that perfect central complementarity was not required for strong silencing. Furthermore, they appraised differences in the miRNA : target mRNA stoichiometry and the context in which the miRNA binding site resides as key determinants in controlling the degree of silencing (Li *et al.*, 2014; Todesco *et al.*, 2010). The putative miR399 binding site within TRV RNA1 includes one mismatch at the 5′ seed region and one mismatch and three non-canonical G : U pairs at the 3′ end. Although the miR399–TRV pairing apparently satisfies the canonical parameters for miRNA target recognition (Brodersen & Voinnet, 2009; Palatnik *et al.*, 2003; Schwab *et al.*, 2005), the complementarity is only partial. It is important to bear in mind that, in our experimental conditions, elevated miR172 and miR399 levels in the infiltrated area may boost targeting efficiency under suboptimal miRNA–target complementarity (Li *et al.*, 2014; Todesco *et al.*, 2010).

The challenge ahead is to investigate whether host miRNAs target genuine viral sequences in the context of the infection. Two lines of evidence are in support of this idea. First, *Arabidopsis* miRNAs negatively regulate plant virus chimeras bearing miRNA target sequences (Simón-Mateo & García, 2006). Secondly, *Arabidopsis* plants transformed with recombinant miRNA precursors engineered to contain complementary viral sequences become specifically immune to infection with these viruses (Lin *et al.*, 2009; Niu *et al.*, 2006). Under natural conditions, however, it is still unclear whether interactions involving naturally occurring miRNAs and viral genomes have petty effects on the infection or whether, in contrast, they have a dynamic role in avoiding excessive virus proliferation during infection (Qu *et al.*, 2008). We cannot rule out the possibility that fortuitous interactions between functional miRNAs and viral sequences encoding indispensable functional domains could contribute to shape the outcome of certain plant–virus pathosystems. However, the observation that viruses rapidly evolve their genomes in order to avoid miRNA recognition argues against the efficacy of miRNAs as antiviral regulators in plants (Lin *et al.*, 2009; Simón-Mateo & García, 2006).

METHODS

Plant material and transient expression assay. Transient expression was conducted in *N. benthamiana* plants grown under 16/8 h light/dark and 25 °C. *Arabidopsis* plants were grown under 16/8 h light/dark at 19–22 °C. The *Arabidopsis* homozygous *ago1-27*, *ago2-1* and *ago4-2* were donated by James C. Carrington (The Donald Danforth Plant Center, MO, USA). TRV inoculation of *Arabidopsis* was done as described previously (Fernández-Calvino *et al.*, 2014).

Agroinfiltration of *N. benthamiana* leaves was performed as described previously (Johansen & Carrington, 2001). Unless otherwise indicated, cultures containing GFP-based constructs were infiltrated at OD_{600} 0.1 or 0.2, viral suppressors at OD_{600} 0.3 and cultures harbouring miRNA constructs at OD_{600} 0.6. Cultures carrying sYFPN- and sYFPC-tagged proteins were co-infiltrated each at OD_{600} 0.2. The final concentration of bacteria was normalized to OD_{600} 0.5 or 1.0 by varying the concentration of cells containing empty vector.

RNA analysis. Total RNA was extracted with TRIzol reagent (Invitrogen). Denaturing gel blot hybridization of normalized total RNA was done as described previously (Martínez-Priego *et al.*, 2008). Radiolabelled DNA probes were synthesized by random priming using [α-^{32}P]dCTP. Oligonucleotides complementary to *Arabidopsis* miRNAs were end-labelled with [γ-^{32}P]ATP. One-step qRT-PCRs using β-tubulin [The *Arabidopsis* Information Resource (TAIR) At1g20010] transcripts for normalization were done as described previously (Fernández-Calvino *et al.*, 2015). A list of primers used in this study is provided in Table S1 (available in the online Supplementary Data).

IP and protein analysis. IP assays were done as described previously (Chapman *et al.*, 2004). Protein extracts were prepared and analysed by immunoblot assay after SDS-PAGE with rabbit anti-GFP or anti-HA antibodies (González *et al.*, 2010; Lakatos *et al.*, 2006). Blotted proteins were detected using commercial HRP-conjugated secondary antibodies and a chemiluminescent substrate (LiteAblot).

Vector DNA constructs for BiFC assays. Proteins were cloned into pROK2-based vectors containing the sYFPN- and sYFPC-terminal halves as described previously (González *et al.*, 2010). The 16K mutants (Δ17, C65/66P and GW/GA) were engineered by conventional PCR site-directed mutagenesis. The coding sequence of AGO1 (TAIR At1g48410) and AGO4 (TAIR At2g27040) were amplified from *Arabidopsis* mRNA. All constructs were authenticated by DNA sequencing.

GFP sensors and miRNA-containing DNA constructs for transient expression assays. The 35S–GFP–miR171.1, 35S–GFP–Cym, 35S–GFP–PoLV, 35S–HA–16K, 35S–P19, 35S–P1/HC-Pro and 35S–miR171a constructs have been described elsewhere (Canto *et al.*, 2006; Giner *et al.*, 2010; Llave *et al.*, 2002; Martínez-Priego *et al.*, 2008; Parizotto *et al.*, 2004). The remaining 35S-driven constructs were produced using the binary vector pSLJ75I55 and then introduced into *Agrobacterium tumefaciens* strain GV2260. For GFP-based constructs, the soluble modified GFP cDNA was PCR amplified using reverse tagged-primers that contained the validated *AP2* (TAIR At4g36920) miRNA target sequence, or the viral complementary sequences as found in the genome of the Tennessee isolate of MCDV (GenBank accession no. NC_003626; coordinates 11628–11648) or the PpK20 isolate of TRV (GenBank accession no NC_003805; coordinates 2418–2437). The MIR158a, MIR172b and MIR399b genes were PCR amplified from *Arabidopsis* genomic DNA using gene-specific primers. All constructs generated were verified by DNA sequencing.

Electrophoretic mobility shift assay. An electrophoretic mobility shift assay was done as described by Csorba & Burgyán (2011) using synthetic siRNAs (5′-CGUACGCGUCACGCGUACGUU-3′ and 5′-CGUACGCGUGACGCGUACGUU-3′) (Sigma) labelled with [γ-^{32}P]ATP.

Confocal microscopy. Plant tissue was imaged using an Olympus SZX12 stereomicroscope and a Leica TCS SP5 inverted confocal microscope with an Argon ion laser. GFP was excited at 488 nm and the emitted light captured at 505–555 nm. YFP was excited at 514 nm, and the emitted light was captured at 525–650 nm.

ACKNOWLEDGEMENTS

This work was supported by the Spanish Ministry of Science and Innovation (MICINN-FEDER funding program) (to C. L.) (grants BIO2006-13107 and BIO2009-12004), the Hungarian Scientific Research Fund (grants OTKA NN 107787 and NN 111024) (to L. L.), and MICINN (grant AGL2008-03482) (to T. C.). L. F.-C. was the recipient of a JAE-Doc Contract from CSIC. I. G.-B. and I. G. were supported by graduate fellowships from MICINN. L. L. was supported by TÁMOP-4.2.2.A11/1/KONV-2012-0035. We thank Livia Donaire, M. Teresa Seisdedos and Mónica Fontenla for technical assistance and critical comments on this manuscript. The authors have no conflicting financial or commercial interests.

REFERENCES

Andika, I. B., Kondo, H., Nishiguchi, M. & Tamada, T. (2012). The cysteine-rich proteins of beet necrotic yellow vein virus and tobacco rattle virus contribute to efficient suppression of silencing in roots. *J Gen Virol* **93**, 1841–1850.

Azevedo, J., Garcia, D., Pontier, D., Ohnesorge, S., Yu, A., Garcia, S., Braun, L., Bergdoll, M., Hakimi, M. A. & other authors (2010). Argonaute quenching and global changes in Dicer homeostasis caused by a pathogen-encoded GW repeat protein. *Genes Dev* **24**, 904–915.

Bhattacharjee, S., Zamora, A., Azhar, M. T., Sacco, M. A., Lambert, L. H. & Moffett, P. (2009). Virus resistance induced by NB-LRR proteins involves Argonaute4-dependent translational control. *Plant J* **58**, 940–951.

Brodersen, P. & Voinnet, O. (2006). The diversity of RNA silencing pathways in plants. *Trends Genet* **22**, 268–280.

Brodersen, P. & Voinnet, O. (2009). Revisiting the principles of microRNA target recognition and mode of action. *Nat Rev Mol Cell Biol* **10**, 141–148.

Burgyán, J. & Havelda, Z. (2011). Viral suppressors of RNA silencing. *Trends Plant Sci* **16**, 265–272.

Canto, T., Uhrig, J. F., Swanson, M., Wright, K. M. & MacFarlane, S. A. (2006). Translocation of Tomato bushy stunt virus P19 protein into the nucleus by ALY proteins compromises its silencing suppressor activity. *J Virol* **80**, 9064–9072.

Carbonell, A. & Carrington, J. C. (2015). Antiviral roles of plant ARGONAUTES. *Curr Opin Plant Biol* **27**, 111–117.

Chapman, E. J., Prokhnevsky, A. I., Gopinath, K., Dolja, V. V. & Carrington, J. C. (2004). Viral RNA silencing suppressors inhibit the microRNA pathway at an intermediate step. *Genes Dev* **18**, 1179–1186.

Chen, X. (2004). A microRNA as a translational repressor of *APETALA2* in *Arabidopsis* flower development. *Science* **303**, 2022–2025.

Ciomperlik, J. J., Omarov, R. T. & Scholthof, H. B. (2011). An antiviral RISC isolated from *Tobacco rattle virus*-infected plants. *Virology* **412**, 117–124.

Csorba, T. & Burgyán, J. (2011). Gel mobility shift assays for RNA binding viral RNAi suppressors. *Methods Mol Biol* **721**, 245–252.

Deng, X., Kelloniemi, J., Haikonen, T., Vuorinen, A. L., Elomaa, P., Teeri, T. H. & Valkonen, J. P. (2013). Modification of *Tobacco rattle virus* RNA1 to serve as a VIGS vector reveals that the 29K movement protein is an RNA silencing suppressor of the virus. *Mol Plant Microbe Interact* **26**, 503–514.

Diao, A., Chen, J., Ye, R., Zheng, T., Yu, S., Antoniw, J. F. & Adams, M. J. (1999). Complete sequence and genome properties of Chinese wheat mosaic virus, a new furovirus from China. *J Gen Virol* **80**, 1141–1145.

Donaire, L., Barajas, D., Martínez-García, B., Martínez-Priego, L., Pagán, I. & Llave, C. (2008). Structural and genetic requirements for the biogenesis of tobacco rattle virus-derived small interfering RNAs. *J Virol* **82**, 5167–5177.

Donald, R. G. & Jackson, A. O. (1994). The barley stripe mosaic virus γb gene encodes a multifunctional cysteine-rich protein that affects pathogenesis. *Plant Cell* **6**, 1593–1606.

Dunoyer, P., Pfeffer, S., Fritsch, C., Hemmer, O., Voinnet, O. & Richards, K. E. (2002). Identification, subcellular localization and some properties of a cysteine-rich suppressor of gene silencing encoded by peanut clump virus. *Plant J* **29**, 555–567.

Fernández-Calvino, L., Osorio, S., Hernández, M. L., Hamada, I. B., del Toro, F. J., Donaire, L., Yu, A., Bustos, R., Fernie, A. R. & other authors (2014). Virus-induced alterations in primary metabolism modulate susceptibility to *Tobacco rattle virus* in Arabidopsis. *Plant Physiol* **166**, 1821–1838.

Fernández-Calvino, L., Guzmán-Benito, I., Del Toro, F. J., Donaire, L., Castro-Sanz, A. B., Ruíz-Ferrer, V. & Llave, C. (2015). Activation of senescence-associated Dark-inducible (DIN) genes during infection contributes to enhanced susceptibility to plant viruses. *Mol Plant Pathol*. doi:10.1111/mpp.12257

Garcia-Ruiz, H., Carbonell, A., Hoyer, J. S., Fahlgren, N., Gilbert, K. B., Takeda, A., Giampetruzzi, A., Garcia Ruiz, M. T., McGinn, M. G. & other authors (2015). Roles and programming of Arabidopsis ARGONAUTE proteins during Turnip mosaic virus infection. *PLoS Pathog* **11**, e1004755.

Ghazala, W., Waltermann, A., Pilot, R., Winter, S. & Varrelmann, M. (2008). Functional characterization and subcellular localization of the 16K cysteine-rich suppressor of gene silencing protein of tobacco rattle virus. *J Gen Virol* **89**, 1748–1758.

Giner, A., Lakatos, L., García-Chapa, M., López-Moya, J. J. & Burgyán, J. (2010). Viral protein inhibits RISC activity by argonaute binding through conserved WG/GW motifs. *PLoS Pathog* **6**, e1000996.

González, I., Martínez, L., Rakitina, D. V., Lewsey, M. G., Atencio, F. A., Llave, C., Kalinina, N. O., Carr, J. P., Palukaitis, P. & Canto, T. (2010). Cucumber mosaic virus 2b protein subcellular targets and interactions: their significance to RNA silencing suppressor activity. *Mol Plant Microbe Interact* **23**, 294–303.

Hamera, S., Song, X., Su, L., Chen, X. & Fang, R. (2012). Cucumber mosaic virus suppressor 2b binds to AGO4-related small RNAs and impairs AGO4 activities. *Plant J* **69**, 104–115.

Johansen, L. K. & Carrington, J. C. (2001). Silencing on the spot. Induction and suppression of RNA silencing in the Agrobacterium-mediated transient expression system. *Plant Physiol* **126**, 930–938.

Jones-Rhoades, M. W. & Bartel, D. P. (2004). Computational identification of plant microRNAs and their targets, including a stress-induced miRNA. *Mol Cell* **14**, 787–799.

Karlowski, W. M., Zielezinski, A., Carrère, J., Pontier, D., Lagrange, T. & Cooke, R. (2010). Genome-wide computational identification of WG/GW Argonaute-binding proteins in Arabidopsis. *Nucleic Acids Res* **38**, 4231–4245.

Kasschau, K. D., Xie, Z., Allen, E., Llave, C., Chapman, E. J., Krizan, K. A. & Carrington, J. C. (2003). P1/HC-Pro, a viral suppressor of RNA silencing, interferes with Arabidopsis development and miRNA unction. *Dev Cell* **4**, 205–217.

Lakatos, L., Csorba, T., Pantaleo, V., Chapman, E. J., Carrington, J. C., Liu, Y. P., Dolja, V. V., Calvino, L. F., López-Moya, J. J. & Burgyán, J. (2006). Small RNA binding is a common strategy to suppress RNA silencing by several viral suppressors. *EMBO J* **25**, 2768–2780.

Li, J., Reichel, M. & Millar, A. A. (2014). Determinants beyond both complementarity and cleavage govern microR159 efficacy in Arabidopsis. *PLoS Genet* **10**, e1004232.

Lin, S. S., Wu, H. W., Elena, S. F., Chen, K. C., Niu, Q. W., Yeh, S. D., Chen, C. C. & Chua, N. H. (2009). Molecular evolution of a viral non-coding sequence under the selective pressure of amiRNA-mediated silencing. *PLoS Pathog* **5**, e1000312.

Liu, D. H., Robinson, D. J., Duncan, G. H. & Harrison, B. D. (1991). Nuclear location of the 16K non-structural protein of tobacco rattle virus. *J Gen Virol* **72**, 1811–1817.

Liu, H., Reavy, B., Swanson, M. & MacFarlane, S. A. (2002). Functional replacement of the tobacco rattle virus cysteine-rich protein by pathogenicity proteins from unrelated plant viruses. *Virology* **298**, 232–239.

Llave, C. (2004). MicroRNAs: more than a role in plant development? *Mol Plant Pathol* **5**, 361–366.

Llave, C., Xie, Z., Kasschau, K. D. & Carrington, J. C. (2002). Cleavage of Scarecrow-like mRNA targets directed by a class of Arabidopsis miRNA. *Science* **297**, 2053–2056.

Ma, X., Nicole, M. C., Meteignier, L. V., Hong, N., Wang, G. & Moffett, P. (2015). Different roles for RNA silencing and RNA processing components in virus recovery and virus-induced gene silencing in plants. *J Exp Bot* **66**, 919–932.

Macfarlane, S. A. (2010). Tobraviruses–plant pathogens and tools for biotechnology. *Mol Plant Pathol* **11**, 577–583.

Martín-Hernández, A. M. & Baulcombe, D. C. (2008). Tobacco rattle virus 16-kilodalton protein encodes a suppressor of RNA silencing that allows transient viral entry in meristems. *J Virol* **82**, 4064–4071.

Martínez-Priego, L., Donaire, L., Barajas, D. & Llave, C. (2008). Silencing suppressor activity of the Tobacco rattle virus-encoded 16-kDa protein and interference with endogenous small RNA-guided regulatory pathways. *Virology* **376**, 346–356.

Niu, Q. W., Lin, S. S., Reyes, J. L., Chen, K. C., Wu, H. W., Yeh, S. D. & Chua, N. H. (2006). Expression of artificial microRNAs in transgenic *Arabidopsis thaliana* confers virus resistance. *Nat Biotechnol* **24**, 1420–1428.

Palatnik, J. F., Allen, E., Wu, X., Schommer, C., Schwab, R., Carrington, J. C. & Weigel, D. (2003). Control of leaf morphogenesis by microRNAs. *Nature* **425**, 257–263.

Pantaleo, V., Szittya, G. & Burgyán, J. (2007). Molecular bases of viral RNA targeting by viral small interfering RNA-programmed RISC. *J Virol* **81**, 3797–3806.

Parizotto, E. A., Dunoyer, P., Rahm, N., Himber, C. & Voinnet, O. (2004). In vivo investigation of the transcription, processing, endonucleolytic activity, and functional relevance of the spatial distribution of a plant miRNA. *Genes Dev* **18**, 2237–2242.

Pérez-Cañamás, M. & Hernández, C. (2015). Key importance of small RNA binding for the activity of a glycine-tryptophan (GW) motif-containing viral suppressor of RNA silencing. *J Biol Chem* **290**, 3106–3120.

Qi, Y., He, X., Wang, X. J., Kohany, O., Jurka, J. & Hannon, G. J. (2006). Distinct catalytic and non-catalytic roles of ARGONAUTE4 in RNA-directed DNA methylation. *Nature* **443**, 1008–1012.

Qu, F., Ye, X. & Morris, T. J. (2008). Arabidopsis DRB4, AGO1, AGO7, and RDR6 participate in a DCL4-initiated antiviral RNA silencing pathway negatively regulated by DCL1. *Proc Natl Acad Sci U S A* **105**, 14732–14737.

Schott, G., Mari-Ordonez, A., Himber, C., Alioua, A., Voinnet, O. & Dunoyer, P. (2012). Differential effects of viral silencing suppressors on siRNA and miRNA loading support the existence of two distinct cellular pools of ARGONAUTE1. *EMBO J* **31**, 2553–2565.

Schwab, R., Palatnik, J. F., Riester, M., Schommer, C., Schmid, M. & Weigel, D. (2005). Specific effects of microRNAs on the plant transcriptome. *Dev Cell* **8**, 517–527.

Silhavy, D., Molnár, A., Lucioli, A., Szittya, G., Hornyik, C., Tavazza, M. & Burgyán, J. (2002). A viral protein suppresses RNA silencing and binds silencing-generated, 21- to 25-nucleotide double-stranded RNAs. *EMBO J* **21**, 3070–3080.

Simón-Mateo, C. & García, J. A. (2006). MicroRNA-guided processing impairs Plum pox virus replication, but the virus readily evolves to escape this silencing mechanism. *J Virol* **80**, 2429–2436.

Szittya, G., Molnár, A., Silhavy, D., Hornyik, C. & Burgyán, J. (2002). Short defective interfering RNAs of tombusviruses are not targeted but trigger post-transcriptional gene silencing against their helper virus. *Plant Cell* **14**, 359–372.

Te, J., Melcher, U., Howard, A. & Verchot-Lubicz, J. (2005). Soilborne wheat mosaic virus (SBWMV) 19K protein belongs to a class of cysteine rich proteins that suppress RNA silencing. *Virol J* **2**, 18.

Todesco, M., Rubio-Somoza, I., Paz-Ares, J. & Weigel, D. (2010). A collection of target mimics for comprehensive analysis of microRNA function in *Arabidopsis thaliana*. *PLoS Genet* **6**, e1001031.

Vaucheret, H. (2008). Plant ARGONAUTES. *Trends Plant Sci* **13**, 350–358.

Yelina, N. E., Savenkov, E. I., Solovyev, A. G., Morozov, S. Y. & Valkonen, J. P. (2002). Long-distance movement, virulence, and RNA silencing suppression controlled by a single protein in hordei- and potyviruses: complementary functions between virus families. *J Virol* **76**, 12981–12991.